CELL-INTEGRATED SENSING FUNCTIONALITIES FOR SMART BATTERY SYSTEMS WITH IMPROVED PERFORMANCE AND SAFETY

GA 957273

D4.5 ADVANCED STATE ESTIMATION ALGORITHMS BASED ON LEVEL 2 SENSORS

LC-BAT-13-2020 - Sensing functionalities for smart battery cell chemistries

Deliverable No.	D4.5	
Related WP	WP4	
Deliverable Title	Advanced state estimation algorithms based on level 2 sensors	
Deliverable Date	15-12-2023	
Deliverable Type	REPORT	
Dissemination level	Public (PU)	
Written By	Francis le Roux (TU/e) Henk Jan Bergveld (TU/e, NXP-NL) Sebastiano Bellani (BDM)	10-11-2023 05-12-2023 23-11-2023
Checked by	Joris de Hoog (FM)	05-12-2023
Reviewed by	Inigo Gandiaga (IKE) Martin Wenger (FHG)	08-12-2023 08-12-2023
Approved by	Inigo Gandiaga (IKE)	15-12-2023
Status	Final	15-12-2023

Summary

In the SENSIBAT project, two types of sensor technology have been investigated: the inclusion of integrated thermal and pressure sensors, which the consortium have called Level-1 sensor (L1) and that is discussed in Deliverable 4.4 and the introduction of a reference electrode, called Level-2 sensor (L2). The latter is the topic of this document.

A reference electrode is a third electrode, sandwiched between the anode and cathode, which does not participate in the functional electrochemical process of a lithium-ion battery. In contrast, the reference electrode should provide a stable potential against which the potentials of the anode and cathode can be measured, irrespective of the operating conditions. Also, this stable potential provided by the reference electrode can be exploited to perform Electrochemical Impedance Spectroscopy (EIS) measurements of each half cell separately. EIS measurements with a third electrode enables dynamic characterization of individual electrodes, providing insights into the kinetics of electrochemical reactions. This dynamic information is valuable for state estimation algorithms, allowing them to adapt to changing conditions and improve accuracy in predicting the State of Charge (SoC), State of Health (SoH), and other battery parameters such us the safety of the cell.

This deliverable report describes the EIS measurements performed on individual half cells and their consistency compared to the overall cell impedance. A brief outlook is supplied on how such individual half-cell EIS measurements, besides being applied in R&D activities to study the origin of certain battery behaviour, could be applied in future BMSs. Moreover, this report describes how the application of reference electrode measurements can be used to obtain individual equilibrium and dynamic electrode potentials, and how these electrode potential measurements can be applied to improve the parameter estimation routine of a physics-based battery model. Physics-based battery models are applied in a BMS when more-detailed information is required on internal battery processes. However, with many parameters to be estimated, there is no guarantee that even though the overall cell voltage is accurately described by the physics-based model, the parameters are correct and lead to a correct modelling of the internal processes. This report shows that the parameter estimation process can be improved for the Doyle-Fuller-Newman (DFN) model by exploiting electrode voltage curves enabled by the L2 sensor. The result is a model with similar cell voltage accuracy as when using the original parameter estimation routine, but with a more accurate description of the internal processes since the accuracy of the modelled electrode potentials has increased significantly.

Finally, based on the results obtained in this deliverable, the impact of these results on future state-estimation algorithms is described. Both for having access to individual electrode impedances as well as individual electrode potentials is predicted to have a positive impact on the achieved accuracy of a range of state-estimation algorithms.

Due to the delay in the development of L2-1Ah cells, this deliverable is submitted with four-month delay compared to what is defined in the Annex I of the Grant Agreement (after Amendment approval). This document describes the possible improvements in the lithium-ion battery state estimation based on SENSIBAT L2 sensors. The resulting delay will not lead to further delays in the SENSIBAT project.

Table of Contents

Table of Figures

Abbreviations

Symbol / Abbreviation	
BEV	*Battery Electric Vehicle*
BMS(s)	*Battery Management System(s)*
CC	*Constant Current*
DFN	*Doyle-Fuller-Newman*
DoD	*Depth of Discharge (DoD [%]=100- SoC [%])*
ECM	*Equivalent-Circuit Model*
EIS	*Electrochemical Impedance Spectroscopy*
LFP	*Lithium Iron Phosphate*
L1	*SENSIBAT Level-1 sensor*
L2	*SENSIBAT Level-2 sensor*
OCV (or U)	*Open-Circuit Voltage (equilibrium potential of complete cell)*
OCV_n (or U_n)	*Open-Circuit Voltage of the negative electrode*
OCV_p (or U_p)	*Open-Circuit Voltage of the positive electrode*
PEIS	*Potentiostatic EIS*
RMSE	*Root-Mean-Square Error*
SoC	*State of Charge*
SoE	*State of Energy*
SoH	*State of Health*
SoP	*State of Power*
SoS	*State of Safety*
SoX	*State of X (X can be Charge, Energy, Health, Power or Safety)*
V_{anode}	*Anode voltage (versus ideal 0V)*
$V_{cathode}$	*Cathode voltage (versus ideal 0V)*
V_{cell}	*Cell voltage*
V_{ref}	*Reference voltage (constant 3.41V for all SoC values assumed)*

1 Introduction

In the SENSIBAT project, 1Ah pouch cells were equipped with printed reference electrodes (so-called Level-2 (L2) sensors). In this deliverable report, application of this L2 sensor to obtain a better understanding of the processes occurring at the individual electrodes is achieved by performing Electrochemical Impedance Spectroscopy (EIS) measurements on individual half cells and by using the reference electrode to measure the electrode potentials beyond the already measurable cell voltage.

Chapter 2 refers to the more-detailed deliverables in which the development of the L2 sensors was described. Then, the results of EIS measurements on the individual electrodes are described. It is shown that the impedance of individual half cells is mostly useful for R&D activities, though a short outlook is also given in the application of EIS to be used online in future Battery Management Systems (BMSs) to, e.g., detect internal temperatures, warn for oncoming thermal runaway or Li plating.

Chapter 3 focuses on the use of the L2 sensor to improve the parametrization process of physics-based battery models. Such models contain many model parameters that need to be determined. Typically, this can be done through cell tear down, or through parameter estimation techniques in which the model parameters are determined from input/output data. The informativity of the data plays a large role in the accuracy of the estimated model parameters, and thus the experimental design plays an important role in the parameter estimation routine. By having additional L2 sensor measurements (more data), we improve the informativity of the input/output data which can result in model parameters that not only provide an accurate model output, but also model parameters which are physically meaningful, leading to more accurate modelling of the internal states of the cell.

In chapter 3, we discuss the battery tests implemented for improved parameter estimation of the Doyle-Fuller-Newman (DFN) model through input/output data, as well as how we can use this data to improve the parameter estimation routine through this data. Identifiability of the DFN model remains a key issue, as there are many model parameters that need to be determined, and many combinations of these parameters are possible to achieve the same voltage output of the model. Thus, it is important to improve the parameter estimation routine, in this case by adding L2 sensor data, to ensure that model parameters that are physically meaningful and leading to correctly modelled internal states.

Results of exploiting the L2 sensor to improve the parametrization process of the DFN model are given in chapter 4. It is shown that using individually measured electrode potentials, which becomes possible in L2 cells, similar overall cell voltage accuracy is obtained compared to not using reference electrode measurements, while showing much higher accuracy of the actual electrode potentials. This implies that the parameters yield a physically more meaningful simulation result, which is important when such models are applied for, e.g., aging prediction or battery state estimation in BMS. For example, more accurately modelled electrode potentials also ensure that overpotentials, the driving forces of aging reactions, are modelled more correctly than when parametrizing the model in the state-of-the-art way without access to the individual electrode potentials.

Finally, conclusions are drawn in chapter 5. In this chapter, also an outlook is provided on how the results of this deliverable are predicted to improve future state-estimation algorithms.

2 Electrochemical Impedance Spectroscopy with reference electrode

2.1 Overview of the technology

The development of a printed reference electrode (named L2 sensor) has been described in detail in previous deliverables, namely:

- D2.2: Development of printed electrodes on cell components (separator) [1]
- D2.4: The characterisation of level-2 sensors [2]
- D2.5: The characterisation of pouch cells with integrated level-2 sensors [3]

In addition, deliverable D3.5, entitled "Report prototyping 1 Ah cells with integrated level-2 sensors" [4], describes the activities related to the validation of the L2 sensor functionalities into prototype pouch cells with 1Ah capacity by the responsible partners, ABEE and VAR.

Overall, in the SENSIBAT project, a cell configuration with a reference electrode printed on the separator has been developed, with the aim of improving our understanding of internal processes and electrochemical characteristics of Li-ion battery cells in *operando*. One technique that is enabled by the reference electrode is artifact-free half-cell Electrochemical Impedance Spectroscopy (EIS), where both positive and negative half cells are characterized independently from each other in terms of impedance. The other technique enabled by the reference electrode, also discussed in chapters 3 and 4, is the monitoring of the individual electrode potentials against the reference electrode during battery operation (*i.e.*, dynamic conditions). Both these techniques have been investigated and are demonstrated in this deliverable report. Figure 1 shows the three-electrode pouch cell, as well as a schematical overview of the compositional elements of the investigated pouch cell.

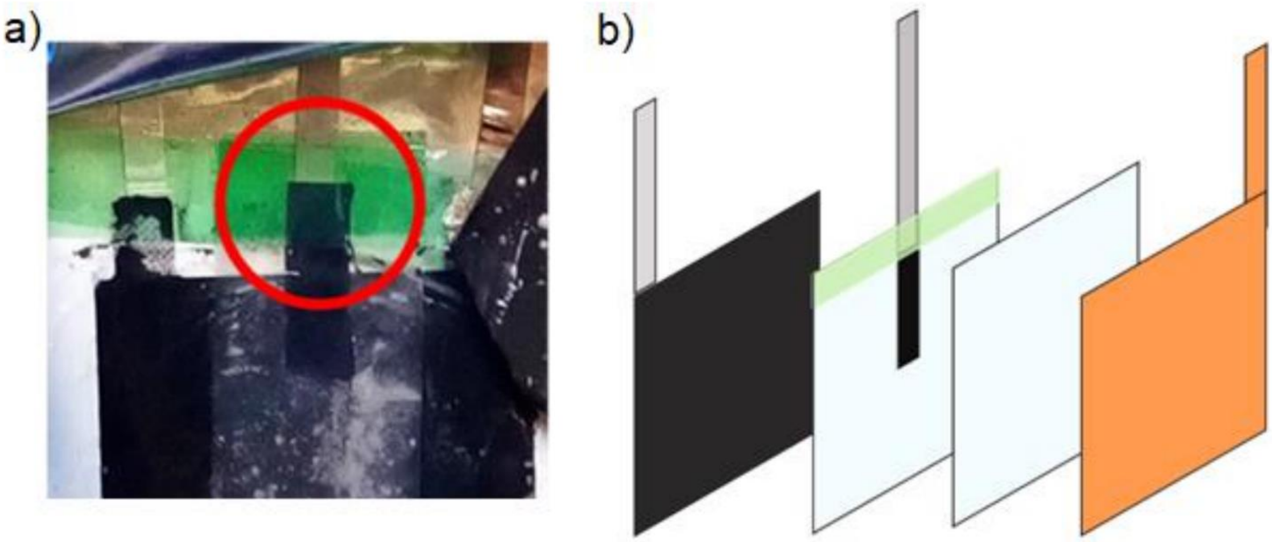

Figure 1: a) Photograph of the three-electrode pouch cell, focusing on the strapping tape and reference electrode regions. b) Sketch of the three-electrode pouch-cell configuration. From left to right: NMC622 cathode, reference electrode printed on Celgard 2500 membrane, Celgard 2500 membrane, graphite anode. Reprinted from the Sensibat D2.5 document.

2.2 EIS measurement results

The EIS measurements were performed using the test definitions described in the SENSIBAT deliverable D1.2 "Testing plan for cells and modules" which are presented in Table 1 [5]. Potentiostatic EIS (PEIS) with a peak-to-peak amplitude of 10mV has been used. During the first charge of the cell, PEIS is performed at SoC values at 10%, 50% and 90% SoC. By subsequently discharging the cell to similar SoC values, PEIS is performed at DoD values of 10%, 50% and 90% (where, DoD [%]=100%-SoC [%]).

Table 1: EIS test plan (repeated from deliverable D1.2 [5]).

Step	Action
1	Constant current (CC) charge at 0.2C, constant voltage at maximum cell voltage
2	CC discharge at 0.2C
3	Repeat step 1 and 2 for 9 times
4	CC charge at 0.2C until 10% of the nominal cell capacity (SoC=10%)
5	Rest 30 min
6	PEIS at 10%
7	CC charge at 0.2C until 50% of nominal cell capacity (SoC=50%)
8	Rest 30 min
9	PEIS at 50% SoC
10	CC charge with 0.2C until 90% of nominal cell capacity (SoC=90%)
11	Rest 30 min
12	PEIS at 90% SoC
13	CC charge at 0.2C until maximum voltage
14	CC discharge at 0.2C until 90% of nominal cell capacity (SoC=90%, DoD=10%)
15	Rest 30 min
16	PEIS at 90% SoC
17	CC discharge at 0.2C until 50% of nominal cell capacity (SoC=50%, DoD=50%)
18	Rest 30 min
19	PEIS at 50% SoC
20	CC discharge at 0.2C until 10% of nominal cell capacity (SoC=10%, DoD=90%)
21	Rest 30 min
22	PEIS at 10% SoC
23	CC discharge at 0.2C until minimum cell voltage

The results of this test plan are shown in Figure 2, which shows the impedances of the individual half cells (NMC 622 cathode and graphite anode) versus the lithium-iron-phosphate (LFP)-based reference electrode, as well as the full cell impedance, obtained by summing the two half-cell impedances. The results show that the overall cell impedance of the pouch cells (blue curves) increase when the SoC decreases (DoD increases) (Figure 2a and f), especially for the impedance related to the lowest-frequency semicircle. This information has also been reported in the SENSIBAT Deliverable 2.5 and has been repeated in this document. At high SoC (low DoD) (Figure 2 c and d), the impedance of the positive half cell (black curves) is significantly smaller than that recorded at low SoC (high DoD). Also, the Nyquist plot of negative half cell (purple curves) reveals the presence of a low-frequency hook (also called inductive loop, curl-back or negative loop) that has been explained from a systems-theory perspective in specific literature, excluding measurement artifacts [6],[7]. In accordance with literature, the low-frequency hook is observed for all the investigated entire SoC (DoD) values [6]. The inductive behaviour of graphite-based half cells has been associated with multiple impedance contributions, including electrolyte impedance and the impedances related to charge-transport kinetics and solid-state diffusion processes in the cells. As stated in [6], since the kinetics and solid-state diffusion processes can be different in different cell assemblies and configurations, the cell assembly and configuration can play an important role in the presence of the inductive loop and, generally, EIS measurements and analysis. These data highlight the powerful feature of the refence electrode to remark specific impedance features of the individual half cells, enabling extensive understanding of each electrode's electrochemical processes and transport phenomena. This data can then be used to improve the cell assembly and configuration for optimum performance of the overall cell.

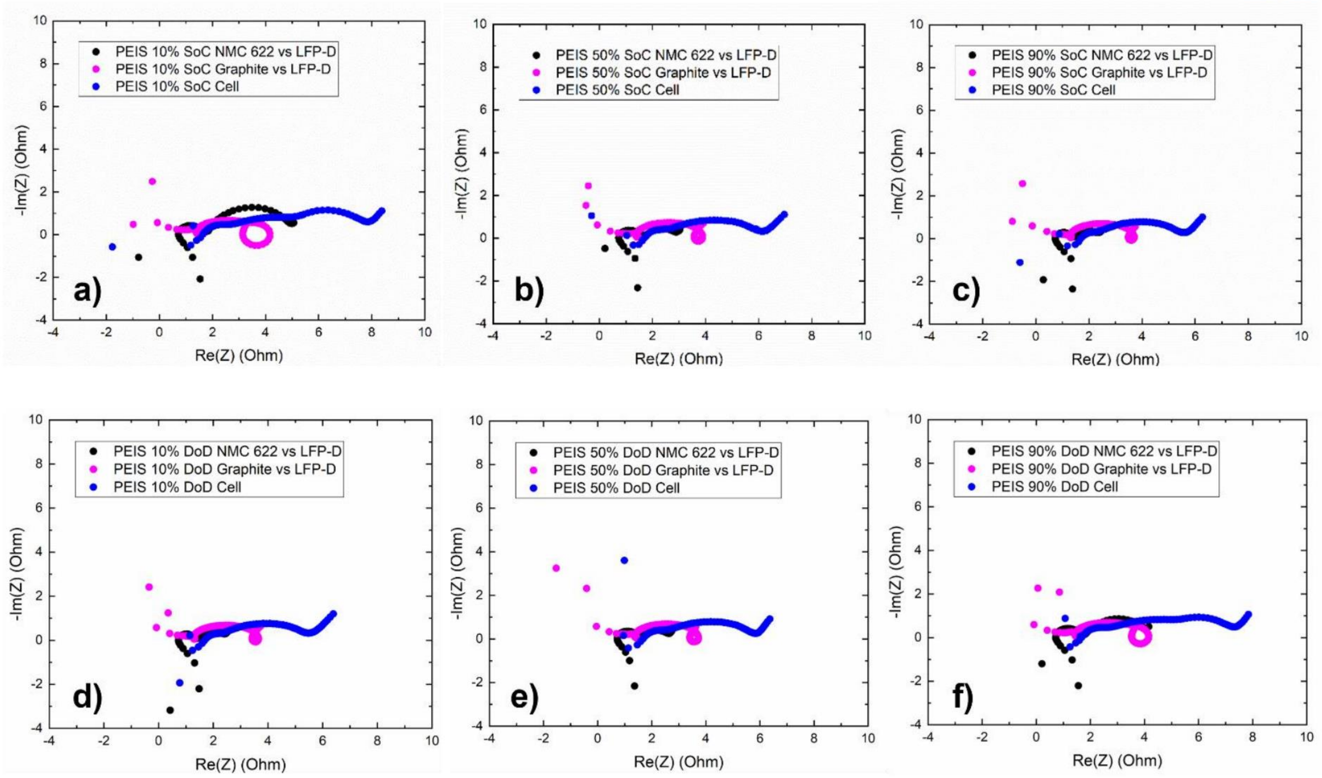

Figure 2: Nyquist plots of the half cells (black dots: NMC cathode versus LFP reference electrode, purple dots: graphite anode versus LFP reference electrode) at a)10% SoC, b) 50% SoC, c) 90% SoC, d) 10% DoD, e) 50% DoD, f) 90% DoD, measured for a representative three-electrode pouch cell configuration using an LFP-D reference electrode. The full cell impedance, obtained by the sum of the impedances of the two half cells, is also shown (blue dots).

To further investigate the consistency of the individual electrode impedances measured using the reference electrode, at different SoC and DoD values, PEIS data measured between cathode and anode for a two-electrode pouch cell were compared with those measured for a three-electrode pouch cell incorporating the reference electrode. The PEIS data for the latter case were computed by summing the impedance recorded for the half-cell configurations, as already shown in Figure 2. As shown in Figure 3: Nyquist plots measured for a two electrode-pouch cell (black dots) and the Nyquist plot corresponding to sum of the half-cell impedances measured in three-electrode pouch cell using LTO-D reference electrode (red dots), at various SoCs and DoDs: a)10% SoC, b) 50% SoC, c) 90% SoC, d) 10% DoD, e) 50% DoD, f) 90% DoD. for all the analysed SoC and DoD values, the PEIS spectra for the two different pouch cell configurations are comparable. Thus, these data support that the reference electrode has marginal impedance contribution to the overall cell impedance, which is consistent with the reference electrode modelling reported in the D2.4 deliverable [3]. Therefore, the compensation methods described in [8], chapter 7, to avoid measurement artifacts leading to erroneous data interpretations, are not necessary in this case. Nevertheless, our EIS data remark remains that it is still complicated to implement universal procedures to analyse impedance spectra and, in particular, to correlate EIS data to battery parameters. Therefore, as also advised by the SENSIBAT Advisory Board, EIS analysis through the proposed reference electrodes has major importance for acquiring knowledge in R&D activities rather than for the development of advanced BMS algorithms for battery state estimation. Still, a brief outlook of how EIS data can be applied in an actual BMS is described in the next section.

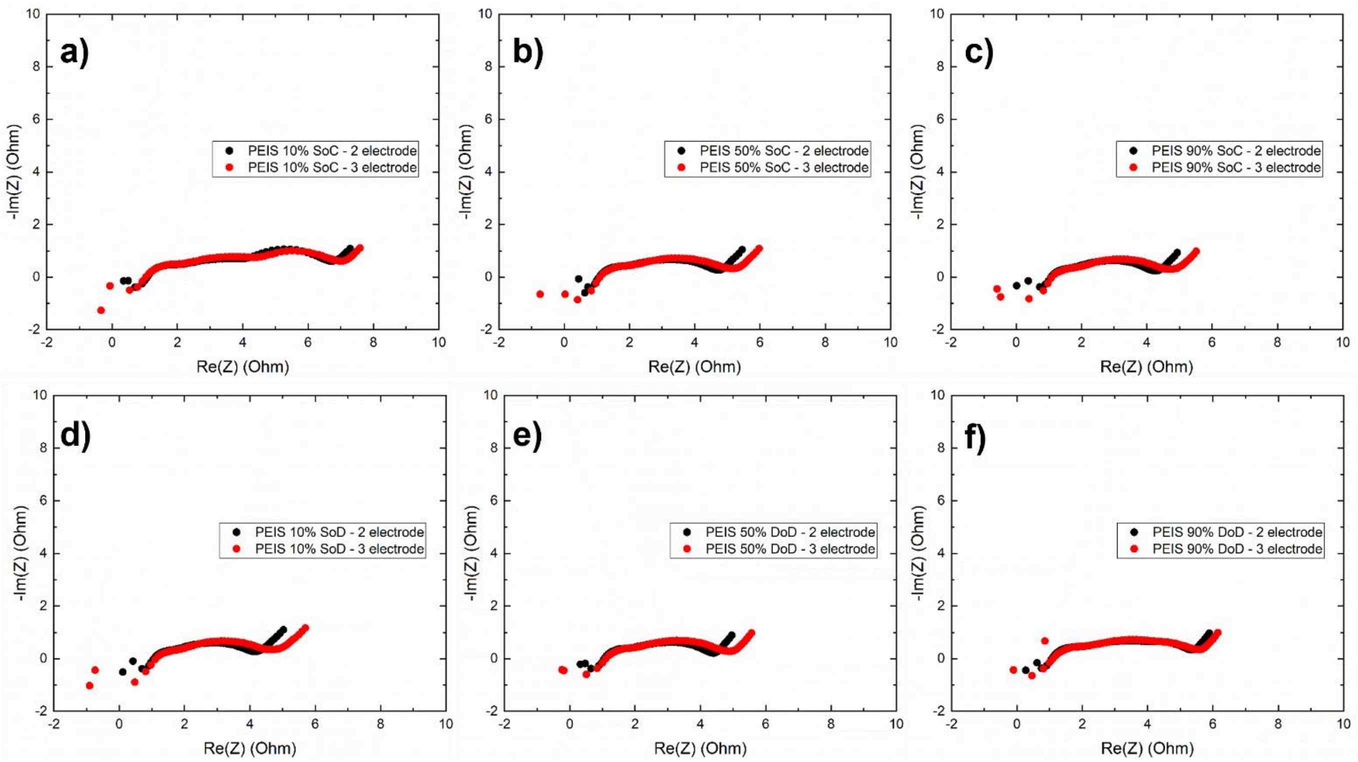

Figure 3: Nyquist plots measured for a two electrode-pouch cell (black dots) and the Nyquist plot corresponding to sum of the half-cell impedances measured in three-electrode pouch cell using LTO-D reference electrode (red dots), at various SoCs and DoDs: a)10% SoC, b) 50% SoC, c) 90% SoC, d) 10% DoD, e) 50% DoD, f) 90% DoD.

2.3 EIS potential in future BMS

The application of EIS in an actual BMS is a continuous topic for research. A good overview paper of potential application of EIS in BMS is given in [9]. As is shown in [9], most studies focus on linking a measured impedance to a certain process in a laboratory environment (R&D activities), and not many papers describe the actual application of EIS in BMS, e.g., in a running electric vehicle. For the latter, many other practical problems exist, such as achieving an acceptable signal-to-noise ratio of the measurement, especially when many disturbances are around, dealing with crosstalk from current-carrying wires to sense wires which influences the measurements, etc. Some examples of how to address these issues when applying EIS for internal temperature assessment is given in [8] and the papers referred to therein.

The measurements presented in this chapter yield individual half-cell impedances that can help to shed light on how certain battery processes inside the two electrodes can be related to the measured impedance. A good overview of applying EIS to assess the internal temperature of a cell is given in [10]. In related work, it is shown that by having access to the impedances of individual half cells, by exploiting a reference electrode, the temperature dependence of the individual electrodes can be studied, which enables using specific half-cell impedances to infer temperature, depending on which half-cell is dominant [8]. Other applications that are currently under investigation are the prediction of thermal runaway [11] or the onset of Li plating [12]. Especially for the latter case, where trends in the real and imaginary part of the overall cell impedance are exploited to predict the onset of Li plating, having access to the individual half-cell impedances may help to see the onset of plating even better. For sure, having access to the electrode potentials, so also the anode potential, helps to infer that plating occurs, i.e., when the anode potential drops below 0 V vs. Li/Li^+. Another example of exploiting separate electrode measurements is given in the next chapter.

3 Experimental design for improved parameter estimation of the DFN model by incorporating reference electrode measurements

In this chapter, a number of experiments is described that were conducted on the L2 cell, to determine if the addition of a reference electrode measurement results in model parameters of a physics-based battery model, such as the Doyle-Fuller-Newman (DFN) model, that are physically more meaningful. These experiments included pulse discharge tests, which would be used to determine the electrode open-circuit voltage (OCV) curves, and drive cycles, which replicate a drive cycle in a Battery Electric Vehicle (BEV). First, some basic information on the applied physics-based model is given, after which the experiments are described.

3.1 Doyle-Fuller-Newman battery model

The application of physics-based models in a BMS is another important topic in battery research. In general, physics-based models are used in a BMS in case more-detailed information on the internal states of a battery is needed in the control of how the battery is used. An example is aging-aware charging, in which case a physics-based model is used to describe not only the regular electrochemical reactions taking place in the cell, but also the aging reactions [13]. The example of applying a physics-based model to aging-aware charging as in [13] is done using the so-called Doyle-Fuller-Newman (DFN) model [14] with added aging reactions. The DFN model is an electrochemistry-based model of Li-ion battery technology that describes concentrations and potentials in two dimensions, the radial and longitudinal dimension.

For a senseful physics-based model, it is important that it not only correctly predicts the overall cell voltage (for which purpose also an Equivalent-Circuit Model (ECM) could be used), but that this is achieved by providing an accurate representation of what is occurring inside the battery (which is not achieved with an ECM). Besides a good model, which properly describes the relevant processes, it is important to find the right parameter values for this model. Since the DFN model contains many different parameters, finding a unique set of parameter values that properly represents battery behaviour is not trivial. A good example of how regular parameterization of the DFN model could be performed can be found in [15]. In this case, the number of parameters is reduced first, after which the parameters are normalized and a sensitivity analysis is performed to find the most influential parameters by ranking them. For the most sensitive parameters, changing their value in a parameter estimation routine has most influence on the model output, i.e., the cell voltage. Moreover, a so-called synthetic cell is exploited in [15], which is basically a model representing a real battery, where, by adding non-idealities to this synthetic cell, the actual model that is being parametrized on 'measurements' coming from this synthetic cell still differs from the real 'battery' (synthetic cell) it is being parameterized on. Having access to the real parameter values and internal states in the synthetic cell when parametrizing the actual model on it, it is investigated how different parameter sets may lead to the same cell potential, but quite different values of internal states.

In mentioned work [15], a reference electrode reading is not available. Instead, a negative electrode equilibrium potential is assumed from literature, and this assumed negative electrode equilibrium potential (OCV_n) is subtracted from the overall obtained battery equilibrium potential OCV curve to obtain the positive electrode equilibrium potential (OCV_p). With the availability of the L2 sensors, however, it becomes possible to exploit the availability of measured positive and negative electrode potentials in the parameter estimation process. The experiments that were performed exploiting the L2 sensor in the parametrization process are described in the next sections.

3.2 Hybrid Pulse Discharge Tests for determination of electrode potential curves

In order to obtain the electrode potential curves, we need to relate the OCV of the cell to the State-of-Charge (SoC). Such an OCV curve forms the thermodynamical basis of the DFN model, where individual electrode OCV curves (OCV_n and OCV_p) need to be derived from this overall cell OCV curve. We can do this by allowing the cell to discharge through applied pulses, with a rest period after each pulse which allows the cell voltage to recover to a relaxed state which corresponds to the equilibrium potential or OCV (Figure 4). These measurements were performed at AIT and the results were processed by TUE.

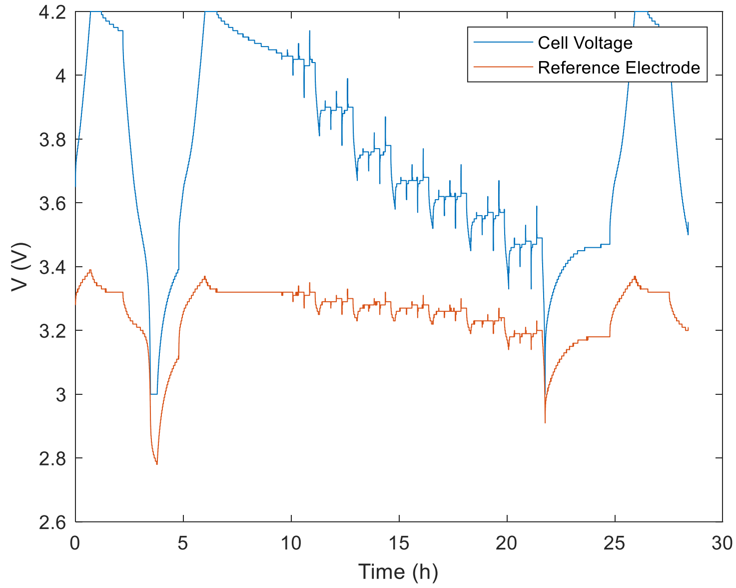

Figure 4: Measured voltage response of the overall cell (blue) and measured reference-electrode-versus-anode voltage response (red) for applied Hybrid Pulse Discharge Testing.

To obtain the potential response of each individual electrode, the cell voltage is measured (blue curve in Figure 4), as well as the response of the reference electrode versus the anode (red curve in Figure 4). In an ideal situation, such as the implementation of a lithium reference electrode, the potential of the reference would be zero. In this case, the potential of the LFP reference electrode V_{ref} is known to be 3.41V and assumed to remain constant for all SoC values, and we thus determine the individual response of the anode (versus an ideal 0V reference) by subtracting the measured response of the reference-electrode-versus-anode curve (red curve in Figure 4) from the assumed constant potential of the reference electrode (V_{ref}=3.41V) (V_{ref}-(V_{ref}-V_{anode})=V_{anode}). We then calculate the cathode potential (versus an ideal 0V reference) by adding the determined anode potential to the overall cell voltage response (since V_{cell}=$V_{cathode}$-V_{anode}). This results in the responses of the cell voltage, as well as the corresponding cathode and anode voltages, as reported in Figure 5.

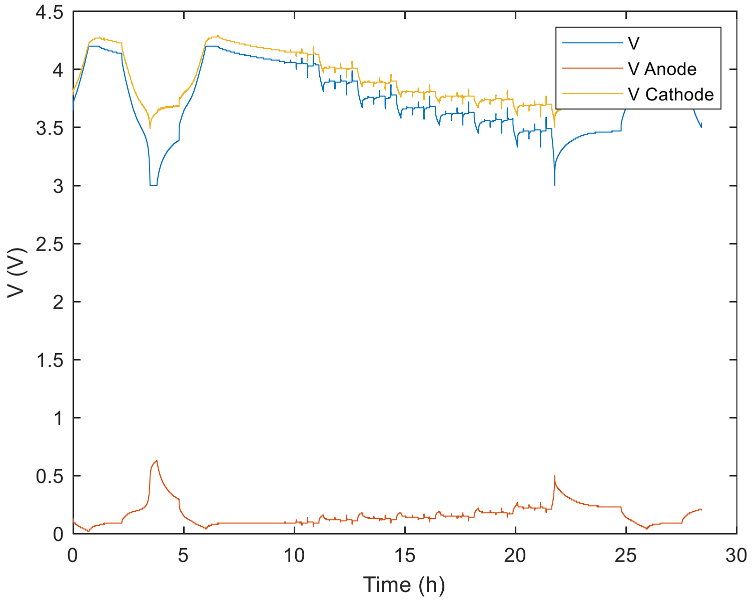

Figure 5: Calculated voltage responses of the anode (red curve) and cathode (yellow curve) (both versus an ideal 0V reference), as well as the measured cell voltage (blue curve) for the Hybrid Pulse Discharge Test.

3.3 Drive-cycle testing for input/output data for the parameter estimation routine

The input/output data required for the parameter estimation routine is in the form of a drive cycle. Such input-output data then relates a dynamic input current (drive cycle) to the measured dynamic output voltage. With the individual electrode OCV curves OCV_n and OCV_p derived from the data in Figure 5 (as will be described in the next chapter, section 4.1), the dynamic input-output data is then used to determine all DFN model parameters. The resulting cell voltage and reference-electrode-versus-anode voltage are shown in Figure 6.

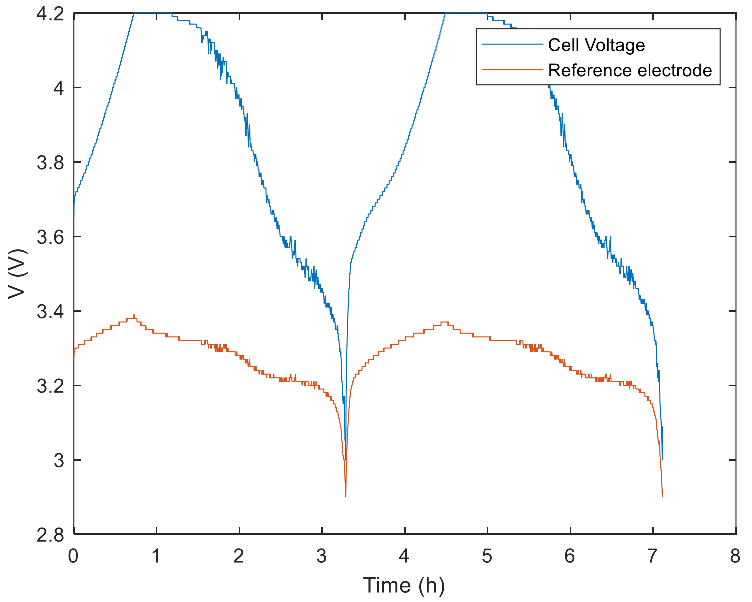

Figure 6: Measured voltage response of the overall cell (blue) and measured reference-electrode-versus-anode voltage response (red) for an applied drive cycle.

In the same manner as for the Hybrid Pulse Discharge tests in section 3.2, the voltage response at each individual electrode (versus an ideal 0V reference) can be determined using the overall cell voltage and measurement of the reference-electrode-versus-anode curve. The determined responses of each individual electrode voltages, as well as overall cell voltage are shown in Figure 7.

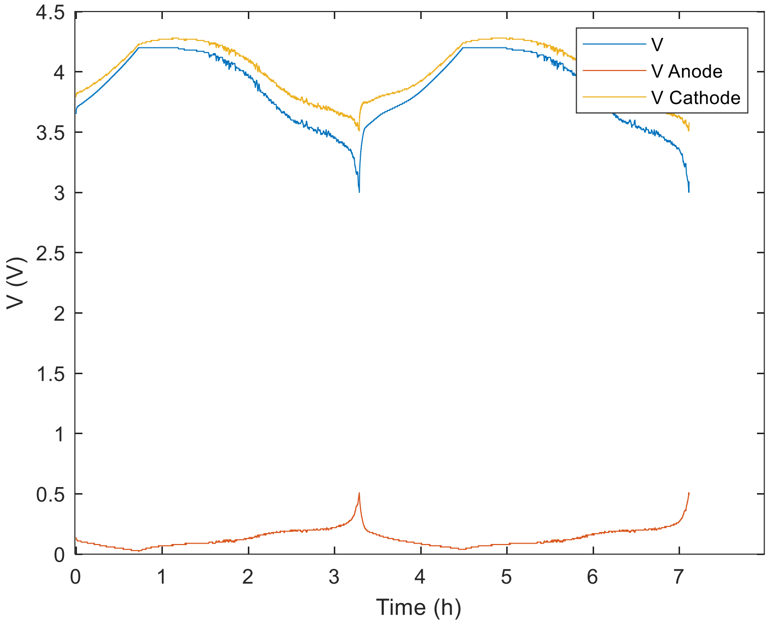

Figure 7: Calculated voltage responses of the anode (red curve) and cathode (yellow curve) (both versus an ideal 0V reference), as well as the measured cell voltage (blue curve) for the drive-cycle test.

4 Methods and results for improved parameter estimation of the DFN model by incorporating reference electrode measurements

4.1 Determination of individual electrode OCV curves by exploiting measurements of a reference electrode

The individual electrode equilibrium potential curves OCV_n and OCV_p can be determined through the implementation of a Hybrid Pulse Discharge Test described in the previous chapter, section 3.2. As described in chapter 3, from the measured cell voltage and reference-electrode-versus-anode voltage curves, the individual anode and cathode potentials (against an ideal 0V reference) can be calculated. Moreover, by fitting a curve through the equilibrium voltages after resting after each discharge pulse has been applied, equilibrium voltages (OCV) of the overall cell (OCV or U in Figure 8), of the anode (OCV_n or U_n in Figure 8) and of the cathode (OCV_p or U_p in Figure 8) can be determined. The resulting equilibrium or OCV curves are shown in Figure 8.

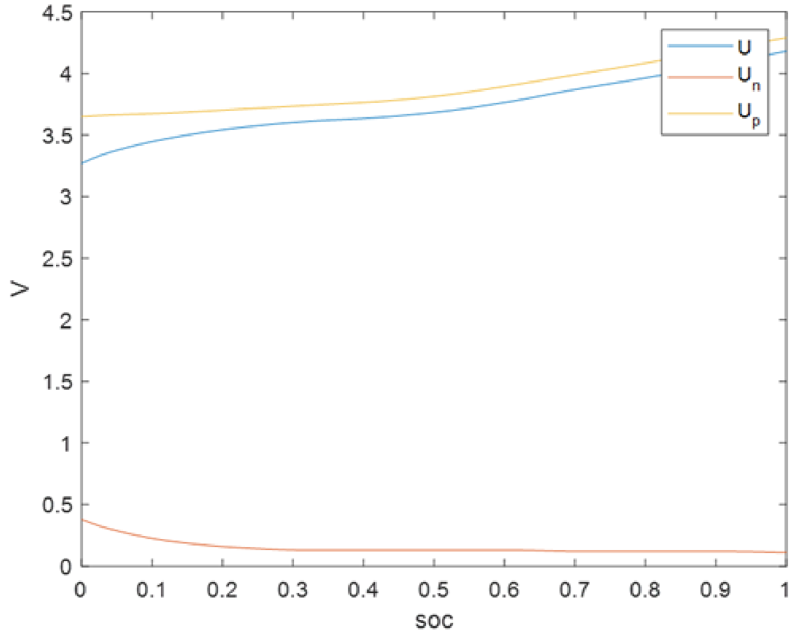

Figure 8: Electrode equilibrium potential curves obtained through measurement: equilibrium cell voltage U (or OCV; blue), equilibrium cathode voltage U_p versus ideal 0V reference (or OCV_p; yellow) and equilibrium anode voltage U_n versus ideal 0V reference (or OCV_n; red).

4.2 Parameter estimation of model parameters with input/output data

To obtain an accurate voltage output of the DFN model, we implement a parameter estimation procedure using input/output data. The parameter estimation procedure is a least-squares optimisation problem that needs to estimate the model parameters while resulting in an accurate voltage output. This procedure can lead to poor identifiability of the model parameters, as there are many model parameters that need to be identified, and many combinations of the model parameters are potentially giving the same model voltage output. One way to address poor identifiability is by improving the informativity of the provided input/output data. The addition of a reference electrode is one such solution, as it allows us to not only have the overall voltage response of the cell, but also the voltage response at each electrode. To quantify the merits of using additional measurement data on individual electrode voltages, a comparison was made between applying the original parameter estimation procedure (where only the overall cell voltage was available) and applying the modified parameter estimation procedure (where besides the overall cell voltage, also the individual electrode potentials were available). The results of the original parameter estimation procedure are shown in Figure 9, while the results of the modified parameter estimation procedure are shown in Figure 10.

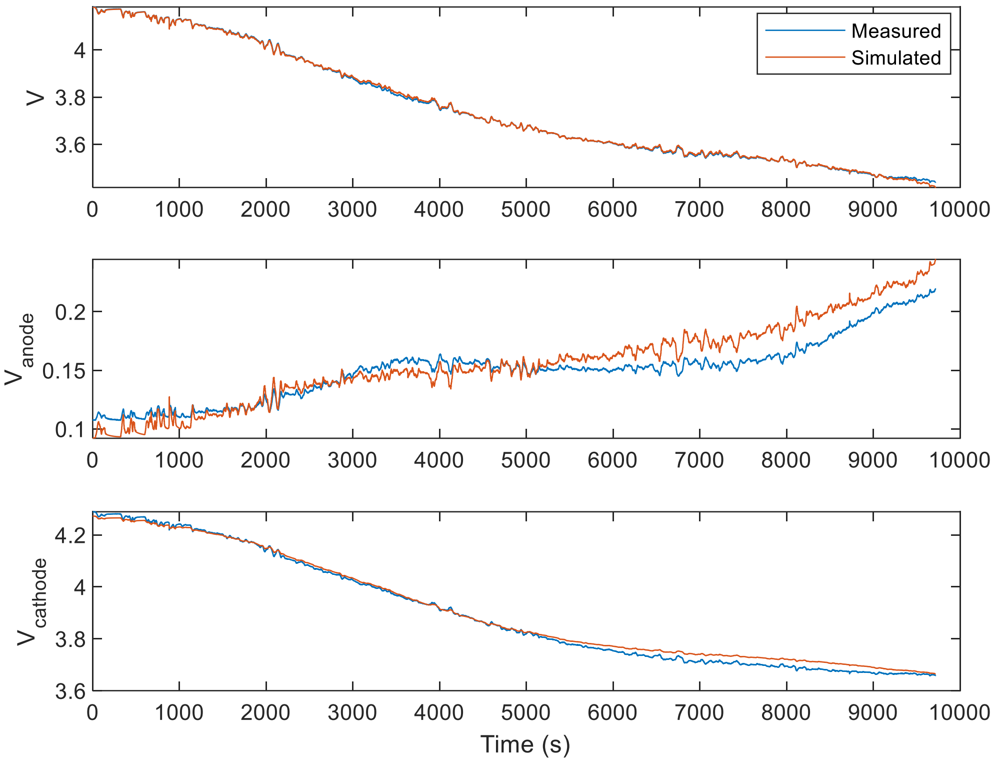

Figure 9: Comparison of measured and simulated voltage responses of the overall cell and respective electrodes (versus an ideal 0V reference) with the original parameter estimation procedure. The measured anode and cathode voltage curves (blue) were NOT used in the parameter estimation routine.

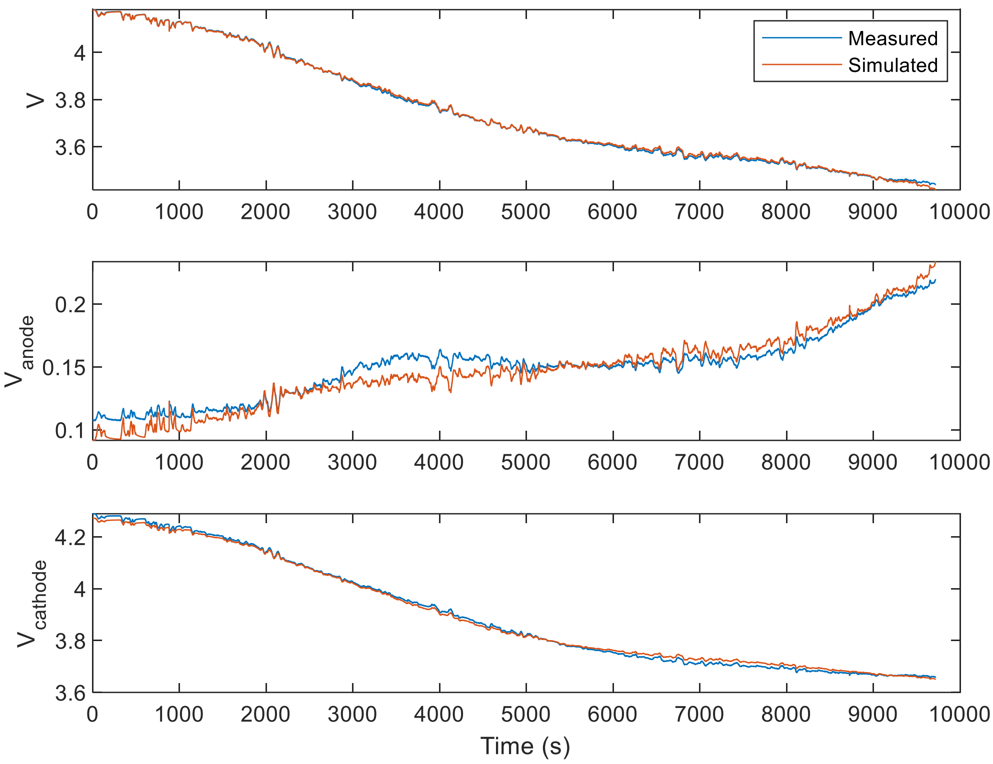

Figure 10: Comparison of measured and simulated voltage Response of the overall cell voltage and respective electrodes (versus an ideal 0V reference) with an adjusted parameter estimation procedure. The measured anode and cathode voltage curves (blue) were used in the parameter estimation routine.

Figure 9 shows the response of measurement and simulation of the voltages of the overall cell and respective electrodes upon the application of a drive cycle for the original parameter estimation procedure. In this estimation, a parameter estimation procedure is performed to estimate the model parameters of the DFN model through input/output data. In this method, no additional reference electrode data is provided in the input/output data and the parameter estimation is only performed on the overall cell voltage response. The negative electrode equilibrium potential curve OCV_n is assumed from literature, after which the positive electrode equilibrium potential curve OCV_p can be calculated by using the overall OCV response of the cell. These OCV_n and OCV_p curves are then used in the DFN model, and all remaining parameters are obtained by applying the mentioned least-squares parameter estimation routine on the overall dynamic cell voltage measured in the drive-cycle experiment. The resulting dynamic cathode and anode voltages (versus an ideal 0V reference) are then compared to the measured dynamic cathode and anode voltages, but these measured cathode and anode voltages were not actively used in the parameter estimation routine.

However, this original parameter estimation routine can be adjusted, with the intention of improving the model voltage response for each individual electrode, which then results in model parameters which are physically more meaningful. In this adjusted method, we include measured electrode equilibrium potential curves to the input/output data (curves U_n and U_p in Figure 8), as well as the measured anode and cathode responses upon application of a drive-cycle to the input/output data (blue measured anode and cathode curves in Figure 10, which are the same as in Figure 9, where these were not actively applied in the parameter estimation routine). Furthermore, we also adjust the model parameters which are being estimated compared to the original parameter estimation routine. Previously, for the results presented in Figure 9, the current collector resistance (one of the DFN model parameters) was estimated as a single model parameter which contained an overall current collector resistance for both current collectors. With the availability of measured individual electrode voltages in the modified parameter estimation routine, this single parameter can now be separated into a current collector resistance for both the anode and the cathode. The voltage responses of the overall cell, of the anode, and the cathode for this modified parameter estimation routine can be seen in Figure 10. It is clear that the overall voltage response remains similar, with an accurate response, but the accuracy of the responses of the individual electrodes clearly improves when additional data is provided to the input/output data. This result provides confidence that the parameter estimation procedure is producing model parameters which are more physically meaningful, and reliable, and having a good representation of the internal states of the cell. For example, when the individual electrode voltages are modelled more accurately, even when leading to the same overall modelled cell output voltage, this leads to the individual reactions, driven by overpotentials that depend on the individual electrode potentials, that are more accurately described. In the end, the sole reason of using a physics-based model like the DFN model is to have a more accurate description of the internal reactions and processes. Therefore, applying the L2 sensor data in the parameter estimation routine of the DFN model helps to ensure proper use can be made of physics-based battery models in a BMS.

In Table 2, we compare the model accuracies of various parameter estimation routines. The original procedure corresponds to the results in Figure 9, where the reference electrode was ignored and only the overall cell voltage was used in the parameter estimation routine. As an intermediate step, the second row corresponds to the situation where the results shown in Figure 8 were used to define the electrode equilibrium potentials in the DFN model (OCV_n or U_n for the anode, OCV_p or U_p for the cathode), but in the actual parameter estimation routine, only the overall cell voltage was used. Finally, the last row corresponds to the results in Figure 10, where besides applying the electrode equilibrium potentials from Figure 8, also the measured dynamic electrode voltages (blue curves in Figure 10) were applied in the parameter estimation routine.

Table 2: Comparison of accuracies (Root-Mean-Square Errors (RMSE)) of measured data vs modelled output for various parameter estimation routines.

Voltage RMSE values [mV]	Cell Voltage	Anode voltage (versus ideal 0V reference)	Cathode voltage (versus ideal 0V reference)
Original Procedure (corresponds to results in Figure 9)	4,52	13,64	16,45
Modified procedure exploiting measured OCV curves OCV_p (U_p) and OCV_n (U_n) only (Figure 8)	6,20	10,58	15,88
Modified procedure exploiting measured OCV curves as well as drive cycles (corresponds to results in Figure 10)	5,49	8,71	9,88

From Table 2, it can be seen that only applying the real measured OCV_n (U_n) and OCV_p (U_p) curves from Figure 8 but not using the measured dynamic electrode potentials (blue measured anode and cathode curves in Figure 9 and Figure 10) makes the overall cell voltage accuracy slightly worse (increase from RMSE of 4.52mV to 6.20mV), while the accuracy of the individual electrode voltages improves slightly. However, when applying the adjusted parameter estimation procedure, where the reference electrode data is used for all input/output data, the model produces comparable accuracies in terms of overall cell voltage (5.49mV versus 4.52mV in the original procedure). However, the most important point to note is the significant improvement of the modelled anode and cathode outputs in this case. By improving these modelled electrode voltage outputs, we can conclude that the model parameters represent the internal states of the cell better, than if no reference electrode data was present.

4.3 Analysis of identifiability of model parameters through a sensitivity analysis

Another way to investigate the difference in identifiability of the original and the modified parameter estimation routine is to perform a sensitivity analysis. We can perform such a sensitivity analysis to understand the sensitivity of the model parameters and the effect that these parameters have on the model output. A sensitivity analysis is a method which measures the sensitivity of the output of a model to the perturbation of the model parameters. In doing so, the analysis provides information regarding which of the model parameters play a bigger role in affecting the model outputs [15].

Figure 11 shows the sensitivity of the model parameters of the DFN model based on the overall voltage response of the cell. This response provides useful information regarding which model parameters are the most sensitive. Parameters that have more impact on the model output (cell voltage in this case), which implies a higher sensitivity on the vertical axis, are ranked higher, so more to the left in the figure. When only the cell voltage is used in the parameter estimation routine, Figure 11 shows which parameters are most important in determining the output and which therefore are most likely to get a realistic value in the parameter estimation routine. As can be seen in the figure, the first parameter related to the positive electrode can be found on rank 3.

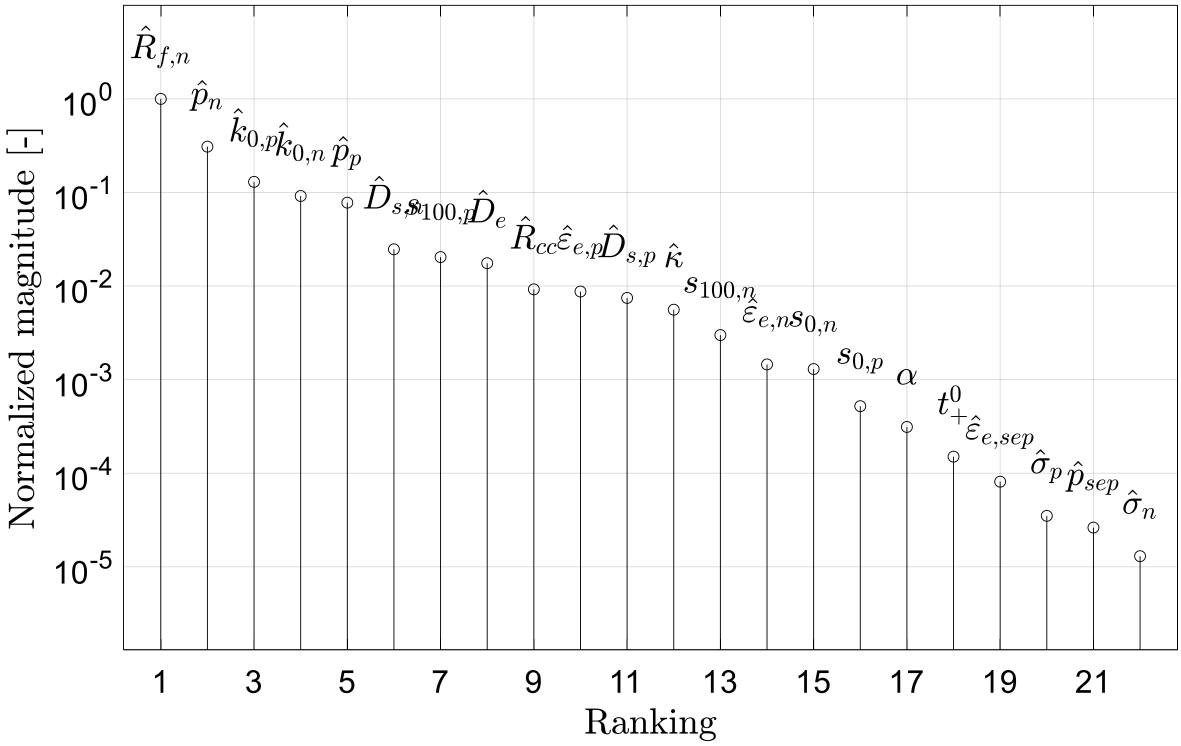

Figure 11: Sensitivity of model parameters of the DFN model to the overall cell voltage.

By performing a sensitivity analysis based on the voltage response at each individual electrode, we obtain more information on the physical meaning of the model parameters, and whether the model parameters affect the output of the model at each electrode as would be expected. Figure 12 shows the sensitivity of the model parameters of the DFN model based on the voltage output of the positive electrode. As can be seen, most of the model parameters with higher sensitivity contain the subscript *p*, indicating that they are the model parameters related to the positive electrode. This means that when taking the individual positive electrode voltage into account in the parameter estimation routine, the actual parameters describing the behaviour of that positive electrode have more impact in the estimation routine and are more likely to get a physically meaningful value. The same can be said for the response at the negative electrode, in Figure 13, where most of the model parameters with a high sensitivity are labelled with subscript *n*. Therefore, the sensitivity analysis described in this section supports that taking individual electrode voltages into account in the parameter estimation routine leads to more meaningful parameters of the DFN model. As mentioned earlier, having more meaningful parameters, and more accurately modelled individual electrode voltages leads to a more accurate representation of internal states. Since this is the main reason for applying physics-based models, such as the DFN model, in a BMS, having the accessibility of L2 sensor outputs results in better models and hence an improved BMS.

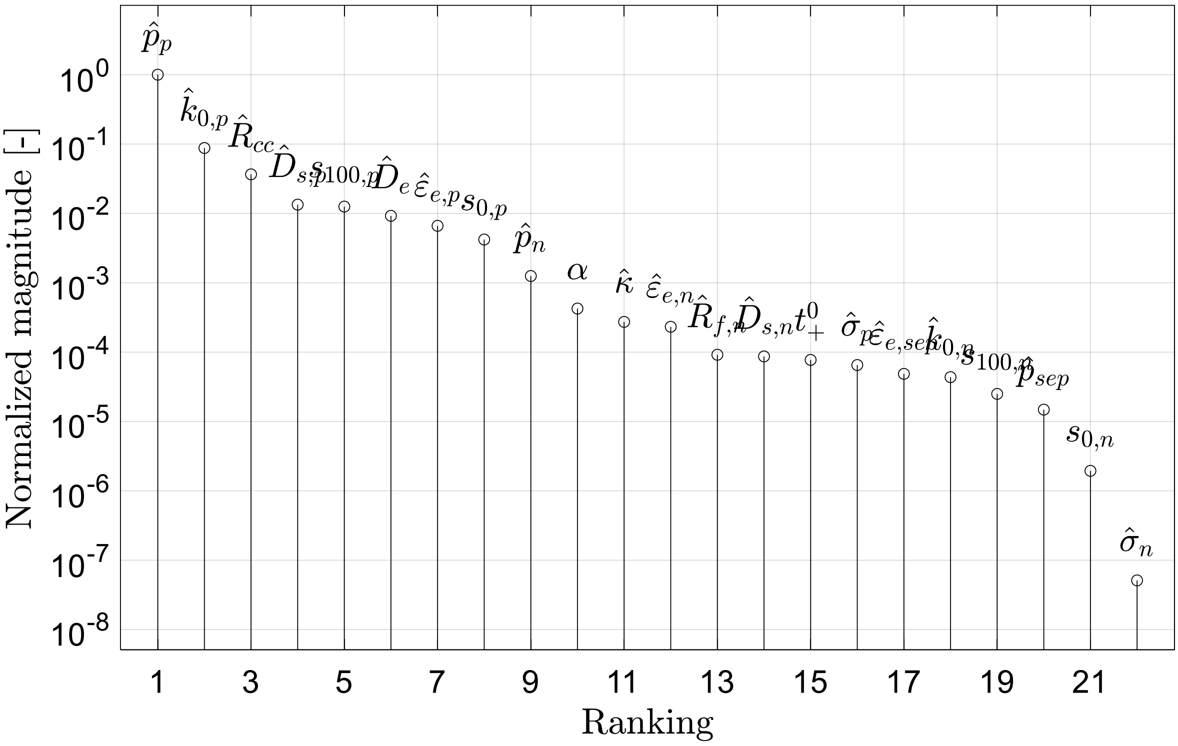

Figure 12: Sensitivity of model parameters of the DFN model to the cathode voltage.

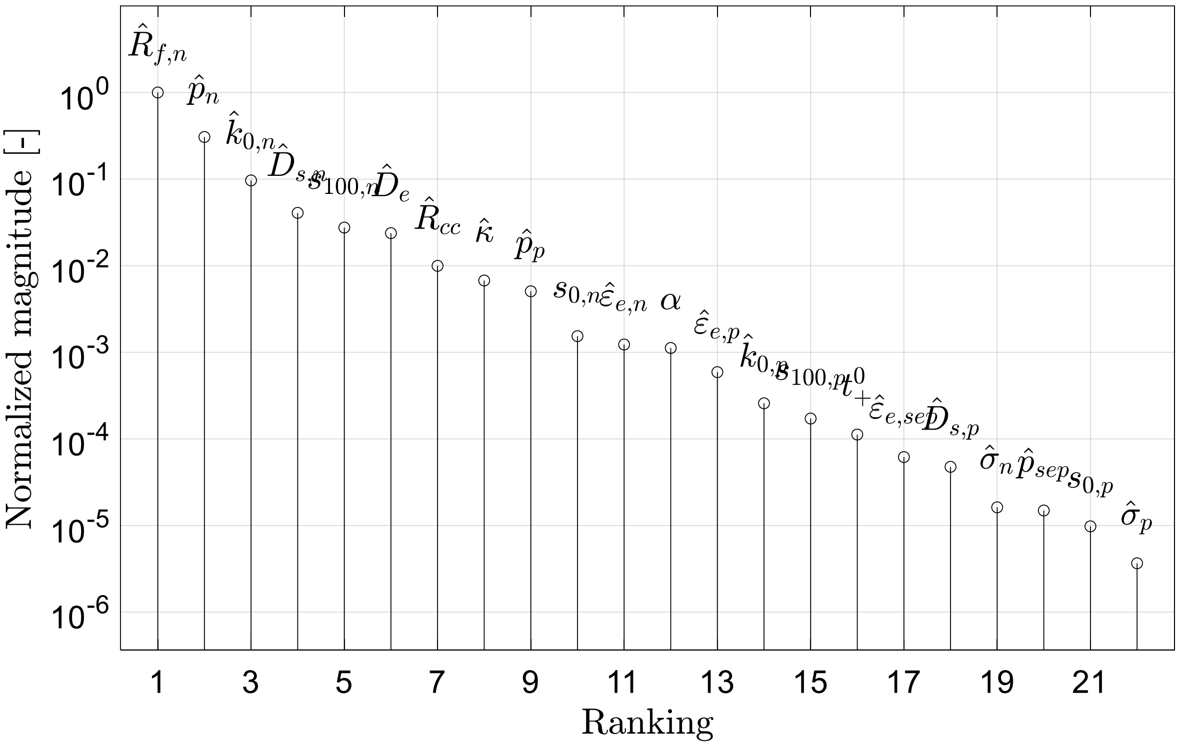

Figure 13: Sensitivity of model parameters of the DFN model to the anode voltage.

5 Discussion & Conclusion

This deliverable report has illustrated two examples of applying the L2 sensor. First, it was shown that it can be used to obtain individual electrode impedances by applying EIS, and secondly, it was described how it can be used to obtain individual electrode voltages, and how those can be used to obtain improved physics-based models. These main contributions are first reflected upon, after which the use of the results of this deliverable in future SoX (SoC, State-of-Health (SoH), State-of-Energy (SoE), State-of-Power (SoP), State-of-Safety (SoS)) algorithms is discussed.

In terms of electrode impedances obtained via EIS, it was shown that different dependencies on SoC and DoD can be seen in the individual electrodes, while addition of the individual electrode impedances, as should be the case, adds up to the overall cell impedance. Since application of EIS using overall cell impedances in actual BMS applications is still in its infancy, applying individual electrode EIS readings in a BMS is even further in the future. For now, the main application of electrode-based EIS is in laboratory environments to obtain more insight in battery behaviour linked to the individual electrodes. As such, this can lead to better cell design. Still, a short outlook is given in chapter 2 on how individual electrode EIS measurements could lead to improved BMS functionality in the future.

This deliverable report also describes how to apply measured individual electrode voltages in the parameter estimation routine for physics-based models, particularly the DFN model. Such a model would be applied in a BMS when more-detailed information about the internal processes and behaviours inside the cell is needed to derive internal states, for example to control charging while minimizing the effect of aging. For something like this to work, it is important that while the model accurately models the cell output voltage (which can be compared to a measured cell voltage in an observer to estimate internal states), the internal states are accurately described. For this to happen, it is important that the parameters, of which there are many in the DFN model, are accurate and have a physical meaning. It is shown in this deliverable report that applying measured electrode equilibrium and dynamic electrode voltages, enabled by the L2 sensor, the accuracy of modelled internal processes is indeed increased, while maintaining similar cell voltage accuracy. Therefore, the L2 sensor can be used during the design phase of the BMS to obtain better models with more meaningful parameters.

In terms of applying the results of this deliverable in future SoX algorithms, we first focus on the availability of electrode-level EIS curves as described in chapter 2.

- State algorithms with a clear relation to impedance could benefit from the availability of the impedance of the individual electrodes, mainly SoH, where the impedance influences the available capacity, and SoP, where the impedance influences the available power. In both cases, knowing which electrode is dominant in determining the impedance may help to make the SoH and SoP algorithms more precise, especially when a physics-based model like the DFN model from chapters 3 and 4 is used including aging reactions at specific electrodes. In that case, knowing the individual electrode impedances may help to tune the parameters of the aging model, where the two electrodes may each include one or more aging reactions, especially those related to increased film resistances [16]. For SoH estimation, knowing the electrode impedances helps to better separate the impedance effect (e.g. due to formed layers) from the capacity loss due to loss of Li ions. Therefore, an increased accuracy of the SoH algorithm will automatically also increase the accuracy of the SoC (which needs an accurate value of the valid capacity in terms of Li ions lost) and therefore also the SoE algorithm.

- Having access to the individual electrode impedances may help to decide which electrode is dominant in determining the internal temperature. A first example of how the internal temperature relates to the individual electrode impedances was given in [8]. In future SoX algorithms, this may be used especially in SoS algorithms to indicate that a particular electrode has become dominant in determining the internal temperature, which may be the first indication of unsafe behaviour. Similarly, when EIS is applied to predict ongoing thermal runaway, or to detect Li plating at the anode, as discussed at the end of chapter 2, doing so with individual electrode impedances may help to make these predictions more precise, thereby increasing the accuracy of the SoS algorithms. An illustration of how L1 sensor readings can be used to improve the SoS algorithm can be found in deliverable report D4.4 [17]. Applying L2 sensor data can be done in a similar manner, where multiplication terms related to the individual electrode impedance measurements can be added.

Focussing on the application of L2 sensors to improve the parameter estimation process of a physics-based battery model as described in chapters 3 and 4, the use of such improved models in future SoX algorithms can be discussed as follows:

- When applying a physics-based model, as described above, the sole reason of doing so is to link an externally measurable variable like cell voltage to internal behaviour. With an improved parameter estimation process, as discussed above, electrode potentials are more accurately modelled, so this also means that overpotentials will be more accurately modelled. As a result, any SoX algorithm relying on an accurate description by the model of what is going on inside the battery will benefit. Particularly, the accuracy of the SoH algorithm based on a physics-based model including aging will improve, simply because the aging model will more accurately describe how capacity is lost and film resistances are increasing. Moreover, e.g. terms can be added to the overall SoS equation as is done in [17] when adding L1 sensor data. When one modelled equation starts to run faster than a certain defined threshold, the corresponding factor in the overall SoS equation can be decreased further, leading to a lower SoS value.
- In the further future, it would also be interesting to not only apply these improved models in a BMS by simply replacing an existing model with the improved model that has been better parametrized, but also apply the measured electrode voltages in an observer in the BMS by comparing them to the modelled values and modifying the estimated internal states accordingly. In this case, feedback in the observer would be determined by more than one feedback signal, which could be exploited to increase the accuracy of SoX algorithms. This would be an interesting topic for further research.

6 References

[1] "SENSIBAT, D2.2: Development of printed electrodes on cell components (separator)", November 2022.

[2] "SENSIBAT, D2.4: The characterisation of level-2 sensors", November 2022.

[3] "SENSIBAT, D2.5: The characterisation of pouch cells with integrated level-2 sensors", 2023.

[4] "SENSIBAT, D3.5: Report prototyping 1 Ah cells with integrated level-2 sensors", 2023.

[5] "SENSIBAT, D1.2 - Testing plan for cells and modules," March 2021.

[6] A. Thapa, H. Gao, "Low-frequency Inductive Loop and Its Origin in the Impedance Spectrum of a Graphite Anode", Journal of the Electrochem. Soc., vol. 169, no. 11, November 2022, 110535.

[7] D. Klotz, "Negative capacitance or inductive loop? – A general assessment of a common low frequency impedance feature", Electrochemistry Communications, vol. 98, January 2019, pp. 58-62.

[8] L.H.J. Raijmakers, "Sensorless Temperature Measurements for Advanced Battery Management Systems", PhD thesis, TU Delft, September 2018.

[9] N. Meddings et al. "Application of electrochemical impedance spectroscopy to commercial Li-ion cells: A review", Journal of Power Sources, vol. 480, 2020.

[10] H. Beelen, et al, "A comparison and accuracy analysis of impedance-based temperature estimation methods for Li-ion batteries", Applied Energy, vol. 175, 2016, pp. 128-140.

[11] P. Dong et al, "Reliable and Early Warning of Lithium-Ion Battery Thermal Runaway Based on Electrochemical Impedance Spectrum", Journal of the Electrochem. Soc., vol. 168, 2021, 090529.

[12] J.P. Schmidt et al, "Time-Resolved and Robust Lithium Plating Detection for Automotive Lithium-Ion Cells with the Potential for Vehicle Application", Batteries, vol. 97, no. 9, January 2023, pp. 1-10.

[13] Z. Khalik, "Modeling and Optimal Control for Aging-Aware Charging of Batteries", PhD thesis, Eindhoven University of Technology, 2021.

[14] M. Doyle, T.F. Fuller, J. Newman, "Modeling of galvanostatic charge and discharge of the lithium/polymer/insertion cell", Journal of the Electrochem. Soc., vol. 140, 1993.

[15] Z. Khalik et al, "Parameter Estimation of the Doyle-Fuller-Newman Model for Lithium-Ion Batteries by Parameter Normalization, Grouping and Sensitivity Analysis", Journal of Power Sources, vol. 449, 2021, 229901.

[16] F. le Roux et al, "Analysis on the Distinguishability of Ageing Mechanisms within a Doyle-Fuller-Newman Framework'', submitted to IEEE American Control Conference (ACC), 2024

[17] "SENSIBAT, D4.4 – ADVANCED MODULE-LEVEL STATE ESTIMATORS BASED ON LEVEL-1 SENSORS," December 2023.

7 Acknowledgement

The author(s) would like to thank the partners in the project for their valuable comments on previous drafts and for performing the review. In particular, Bernd Eschelmüller from AIT is acknowledged for performing the measurements described in chapter 3.

Project partners

#	PARTICIPANT SHORT NAME	PARTNER ORGANISATION NAME	COUNTRY
1	IKE	IKERLAN S. COOP.	Spain
2	BDM	BEDIMENSIONAL SPA	Italy
3	POL	POLITECNICO DI TORINO	Italy
4	FHG	FRAUNHOFER GESELLSCHAFT ZUR FOERDERUNG DER ANGEWANDTEN FORSCHUNG E.V.	Germany
5	FM	FLANDERS MAKE VZW	Belgium
6	TUE	TECHNISCHE UNIVERSITEIT EINDHOVEN	The Netherlands
7	NXP NL	NXP SEMICONDUCTORS NETHERLANDS BV	The Netherlands
8	NXP FR	NXP SEMICONDUCTORS FRANCE SAS	France
9	ABEE	AVESTA BATTERY & ENERGY ENGINEERING	Belgium
10	VAR	VARTA MICRO INNOVATION GMBH	Germany
11	AIT	AIT AUSTRIAN INSTITUTE OF TECHNOLOGY GMBH	Austria
12	UNR	UNIRESEARCH BV	The Netherlands

DISCLAIMER/ ACKNOWLEDGMENT

This project has received funding from the European Union's Horizon 2020 research and innovation programme under grant agreement No 957273. The information and views set out in this publication does not necessarily reflect the official opinion of the European Commission. Neither the European Union institutions and bodies nor any person acting on their behalf, may be held responsible for the use which may be made of the information contained therein.